B. García-Domene; Gomis, O.; F.J. Manjón; H. M. Ortiz; DANIEL ERRANDONEA; DAVID SANTAMARÍA PÉREZ; D. Martinez-Garcia... (2014). Pbca-Type In2O3: The High-Pressure Post-Corundum Phase at Room Temperature. Journal of Physical Chemistry C. 118:20545-20552. doi:10.1021/jp5061599.

Pbca-Type In_2O_3: The High-Pressure Post-Corundum Phase at Room Temperature.

B. García-Domene,[a] J. A. Sans,[b*] O. Gomis,[c] F. J. Manjón,[b] H. M. Ortiz,[b] D. Errandonea,[a] D. Santamaría-Pérez,[a] D. Martínez-García,[a] R. Vilaplana,[c] A. L. J. Pereira,[b] A. Morales-García,[d] P. Rodríguez-Hernández,[e] A. Muñoz,[e] C. Popescu,[f] and A. Segura[a]

[a] ICMUV-Departamento de Física Aplicada, MALTA Consolider Team, Universitat de València 46100 Burjassot, Spain.

[b] Instituto de Diseño para la Fabricación y Producción Automatizada, MALTA Consolider Team, Universitat Politècnica de València 46022 València, Spain.

[c] Centro de Tecnologías Físicas, MALTA Consolider Team, Universitat Politècnica de València 46022 València, Spain.

[d] Departamento de Química-Física I, MALTA Consolider Team, Universidad Complutense de Madrid 28040 Madrid, Spain.

[e] Departamento de Física, MALTA Consolider Team, Universidad de La Laguna 38205 La Laguna, Tenerife, Spain.

[f] ALBA-CELLS 08290 Cerdanyola, Barcelona, Spain.

ABSTRACT: High-pressure powder x-ray diffraction and Raman scattering measurements in cubic bixbyite-type indium oxide (c-In_2O_3) have been performed at room temperature. On increasing pressure c-In_2O_3 undergoes a transition to the Rh_2O_3-II structure but on decreasing pressure Rh_2O_3-II-type In_2O_3 undergoes a transition to a previously unknown phase with Pbca space group which is isostructural to Rh_2O_3-III. On further decrease of pressure, we observed a phase transition to the metastable corundum-type In_2O_3 near room conditions. Recompression of the metastable corundum-type In_2O_3 at room temperature leads to a transition to the Rh_2O_3-III phase, thus showing that the Rh_2O_3-III phase is the post-corundum phase at room temperature. Our results are supported by theoretical *ab initio* calculations. Furthermore, they show that the Rh_2O_3-III phase could be present in other sesquioxides, thus prompting to a revision of the pressure-temperature phase diagrams of sesquioxides

KEYWORDS. high-pressure chemistry • density-functional-calculations • sesquioxides • polymorphism • solid-solid phase transitions.

INTRODUCTION

Indium oxide (In_2O_3) is an attractive sesquioxide employed as a gas sensor,[1-3] in thermoelectrics,[4,5] and specially, when doped with Sn or F, as a transparent conductive oxide in many optoelectronic applications including solar cells, light-emitting diodes, and liquid-crystal displays.[6-9] In_2O_3 crystallizes in the cubic bixbyite (C-type) structure (space group (SG) Ia-3, No. 206, Z=16) and for many years it was known in another metastable structure at ambient conditions, the rhombohedral corundum-type phase (SG R-3c, No. 167, Z=6) which was obtained after application of extreme conditions of pressure and temperature.[10-12] The synthesis of corundum-type In_2O_3 at room conditions[13-18] has allowed the characterization of its properties for its use in industrial applications;[19-21] therefore, the discovery of new phases of this compound is of fundamental and technological interest.

The discovery of the post-perovskite ($CaIrO_3$) phase[22] in $MgSiO_3$ led to a major revision of the pressure-temperature phase diagrams in many ABO_3 compounds including sesquioxides (A=B). Theoretical works in In_2O_3 analyzed several structures and suggested the existence of the post-perovskite phase,[23,24] which, consequently, triggered considerable experimental efforts in order to find this phase at high pressures and high temperatures.[25-29] Noteworthy, experiments showed that the post-perovskite phase is not stable at high pressures in In_2O_3. Instead, two new high-pressure phases were discovered: the orthorhombic Rh_2O_3-II (SG Pbcn, No. 60, Z=4), and the orthorhombic α-Gd_2S_3 phase[25-29] (SG Pnma, No. 62, Z=4). This last phase was initially unexpected and theoretical calculations showed that it was predicted to be the more stable phase[26] at pressures beyond 35 GPa. Hereafter, the cubic, rhombohedral, Rh_2O_3-II and α-Gd_2S_3 phases of In_2O_3 will be named c-In_2O_3, rh-In_2O_3, o1-In_2O_3 and o2-In_2O_3, respectively.

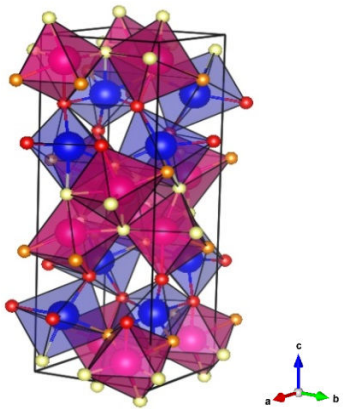

Figure 1. Orthorhombic Pbca-type In_2O_3. Blue and pink atoms represent the two inequivalent In atoms, while red, yellow, and orange atoms represent the three unequivalent O atoms. InO_6 octahedra are shown in the figure.

Recently, several attempts have been performed in order to obtain in a metastable way 01-In_2O_3 at room conditions by means of high pressure and high temperature treatments,[27-29] and a theoretical work has recently commented on the possible applications of 01-In_2O_3.[30] High temperatures have been systematically used in these experimental high-pressure studies in order to induce phase transitions delayed or even impeded in In_2O_3 at room temperature (RT) due to the presence of kinetic effects.[25-29,31] In the last years high-pressure studies of In_2O_3 at RT have also been reported yielding some contradictory results.[32-34] A phase transition from c-In_2O_3 to rh-In_2O_3 between 12 and 25 GPa in bulk and nanocrystalline In_2O_3 was reported,[32,33] whereas no sign of phase transition up to 30 GPa neither in bulk nor in nanocrystalline c-In_2O_3 was found in the latest work[34] in good agreement with previous results.[28]

These contradictory results at high pressure and RT have motivated us to perform a much deeper study of the polymorphism of In_2O_3 at RT up to higher pressures (50 GPa) with both powder x-ray diffraction (XRD) and Raman scattering (RS) measurements. Our work shows that on increasing pressure c-In_2O_3 undergoes a phase transition to 01-In_2O_3 at RT without undergoing a phase transition to rh-In_2O_3. Furthermore, on decreasing pressure we find that 01-In_2O_3 undergoes a phase transition to a previously unknown structure of In_2O_3, the orthorhombic Rh_2O_3-III phase[35] (SG Pbca, No.61, Z=8), hereafter named 03-In_2O_3, prior to the phase transition to rh-In_2O_3, which is the metastable phase at room conditions. Our theoretical *ab initio* calculations suggest that 03-In_2O_3 (see Fig. 1) is competitive in a certain range of pressures with c-In_2O_3, rh-In_2O_3, and 01-In_2O_3. These phases were already theoretically simulated by several authors who did not consider 01-In_2O_3.[26,36]

EXPERIMENTAL SECTION

Bixbyite-type (c-In_2O_3) powders of high purity (99.99%) were commercially obtained from Sigma-Aldrich Inc. On the other hand, corundum-type (rh-In_2O_3) powders were obtained on downstroke from c-In_2O_3 powders pressurized to 50 GPa at RT.

High-pressure angle-dispersive powder XRD experiments at RT up to 50 GPa for c-In_2O_3 and up to 25 GPa for rh-In_2O_3 were conducted in a membrane-type diamond anvil cell (DAC). Either a 16:3:1 methanol-ethanol-water mixture or He gas were used as quasihydrostatic pressure-transmitting media. Pressure inside the DAC was estimated from the EOS of copper.[37] Experiments were performed at the BL04-MSPD beamline of the ALBA synchrotron[38] with an incident monochromatic wavelength of 0.4246 Å focused to 20 x 20 μm. No pinhole was used to cut the x-ray beam tail what explains the presence of the gasket in our XRD patterns. Images covering a 2θ range up to 15º were collected using a SX165 CCD located at 270 mm from sample. One-dimensional diffraction profiles of intensity as a function of 2θ were obtained by integration of observed intensities with the Fit2D software. Lattice parameters of powder XRD patterns were obtained with Rietveld refinements performed using POWDERCELL[39] and GSAS[40] program package.

RS measurements at RT excited either with 532.0 or 632.8 nm laser lines and laser power below 10 mW were performed in a backscattering geometry using a Horiba Jobin-Yvon LabRam HR UV spectrometer in combination with a thermoelectrically-cooled multichannel CCD detector (resolution below 2 cm^{-1}). High-pressure RS measurements in bulk power of c-In_2O_3 up to 50 GPa and of rh-In_2O_3 up to 33 GPa were performed inside the DAC. A 16:3:1 methanol-ethanol-water mixture was used as a pressure-transmitting medium and a few ruby balls of about 2 μm in diameter evenly distributed in the pressure chamber were employed as a pressure sensor.[41]

Ab initio total-energy calculations were performed within the density functional theory using the plane wave method and the pseudopotential theory with the Vienna *ab initio* simulation package (VASP).[42-45] Lattice-dynamics calculations of

the phonons at the zone center (Γ point) of the Brillouin zone were performed using the direct force constant approach. The reader can consult Ref. 34 for further theoretical details.

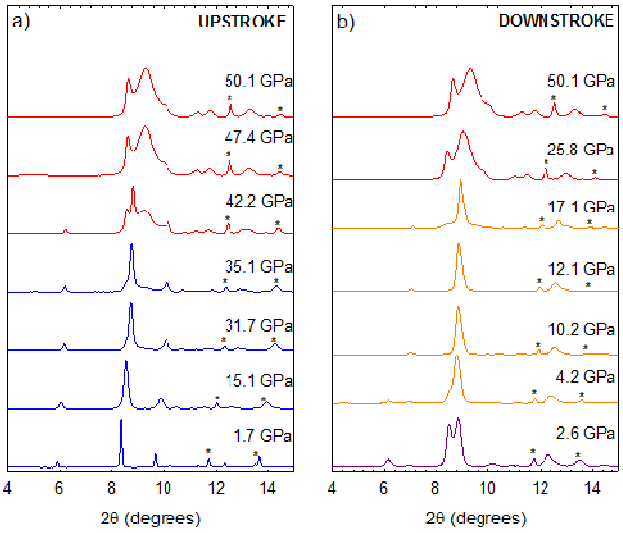

Figure 2. RT-XRD powder patterns of cubic In_2O_3 at selected pressures with helium as pressure-transmitting medium on upstroke up to 50 GPa (a) and on downstroke down to 2.6 GPa (b). Colors indicate the XRD patterns with mainly c-In_2O_3 (blue), o1-In_2O_3 (red), o3-In_2O_3 (orange), and rh-In_2O_3 (violet) phases. Asterisks denote the diffraction maxima of copper at each pressure.

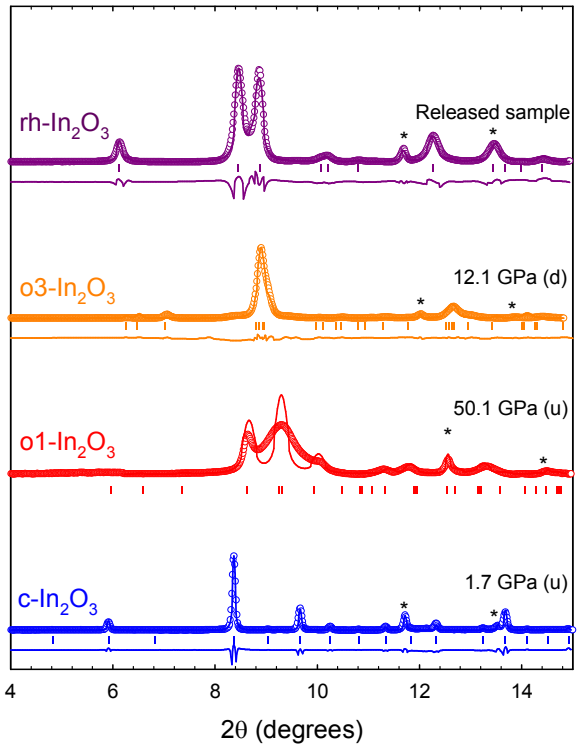

Figure 3. Refinements of the experimental XRD patterns on upstroke (u) at 1.7 GPa with the c-In_2O_3 structure and at 50.1 GPa with the o1-In_2O_3 structure and on downstroke (d) at 12.5 GPa with the o3-In_2O_3 structure and at 1 atm with the rh-In_2O_3 structure. Residuals of the Rietveld refinements are plotted below the experimental (circles) and fitted (lines) XRD profiles (except for o1-In_2O_3 phase, where a LeBail refinement has been performed).

RESULTS AND DISCUSSION

Powder XRD patterns on upstroke up to 50 GPa (Fig. 2a) can be clearly indexed below 35 GPa with the Miller indexes of the Bragg reflections for c-In_2O_3 (see Rietveld refinement of the XRD pattern at 1.7 GPa with Rwp=3.5% in Fig. 3). The onset of a high-pressure phase transition starts above 35.1 GPa. Above 46 GPa the phase transition is completed and the XRD pattern fully corresponds to o1-In_2O_3 (see XRD pattern at 50.1 GPa in Fig. 3) in good agreement with some previous works[25-29] but in disagreement with other works.[32,33] Note that at 50.1 GPa there is a large experimental broadening of the XRD peaks, likely due to the poor crystalline quality of the Pbcn-type phase at high pressures and RT. The peaks obtained by Le Bail refinement agree with the position of the experimental Bragg features but the difference between the widths of both of them causes a big mismatch in the difference spectrum, as we can clearly observe by comparison.

Table 1. Experimental (from Rietveld refinement) and theoretical values of the lattice parameters and atomic positions obtained for the o3 (Pbca) phase of In_2O_3 at 12.1 GPa. Due to the large number of variables, the atomic positions were assumed to be fixed to those theoretically calculated in order to perform a Rietveld refinement of the XRD pattern at 12.1 GPa.

	a (Å)	b (Å)	c (Å)	Atom	Wyckoff site	x	y	z
Experimental	5.380(1)	5.515(1)	15.513(1)	In1	8c	0.0003	0.7887	0.4304
Theoretical	5.433	5.569	15.626	In2	8c	0.9976	0.7352	0.1827
				O1	8c	0.3594	0.8722	0.2014
				O2	8c	0.2063	0.5157	0.3755
				O3	8c	0.1458	0.6550	0.0529

We want to stress that the pressure for the onset of the transition from c-In_2O_3 to o1-In_2O_3 on upstroke decreases with decreasing hydrostatic conditions from 35 GPa with helium to 31 GPa when the experiment was performed with the methanol-ethanol-water mixture. These results clearly indicate that the post-cubic phase of In_2O_3 at RT under reasonable hydrostatic conditions is not the corundum-type phase, as it was assumed in previous works at RT,[32,33] but the orthorhombic Rh_2O_3-II (SG Pbcn) structure. Curiously, our *ab initio* calculations (at T= 0K) indicate that o1-In_2O_3 should be the most stable phase above 8 GPa (see Fig. 4) and below 36 GPa (α-Gd_2S_3 type In_2O_3 is the most stable one above this pressure in good agreement with previous calculations[26,36]). The disagreement between experiments and calculations can be explained by the existence of a high kinetic energy barrier for the transformation from c-In_2O_3 to o1-In_2O_3 as already commented by several authors.[25-29] These high kinetic energy barriers could be studied in future experiments combining pressure with a moderate heating to help the sample to overcome the kinetic barriers in the structural transition.

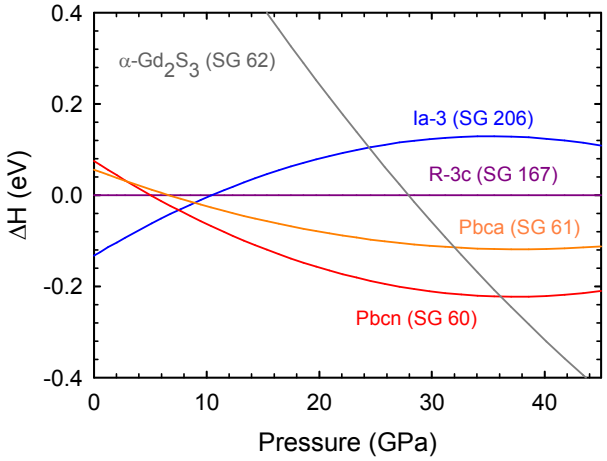

Figure 4. Calculated enthalpy-pressure diagram for In_2O_3 polymorphs with respect to the corundum-type rhombohedral R-3c phase (vilolet): cubic Ia-3 (blue), orthorhombic Pbca (orange), orthorhombic Pbcn (red), and orthorhombic α-Gd_2S_3 (grey). The curve for the P2/c phase goes on top of that of the R-3c phase and it is not plotted.

Powder XRD patterns on downstroke from 50 GPa (Fig. 2b) show that o1-In_2O_3 is stable in the region between 50 and 20 GPa. Below 20 GPa a phase transformation to a previously unknown phase occurs. The XRD pattern at 17.1 GPa corre-

sponds mainly to the new phase with some remnant peaks of o1-In_2O_3. However, at 12.1 GPa the XRD pattern corresponds entirely to the new phase. Finally, on decreasing pressure below 4.2 GPa another phase transition occurs, which resulted in the observation of rh-In_2O_3 at room pressure (see Rietveld refinement in the released sample with Rwp=2.3% in Fig. 3), in good agreement with previously reported results.[27-29]

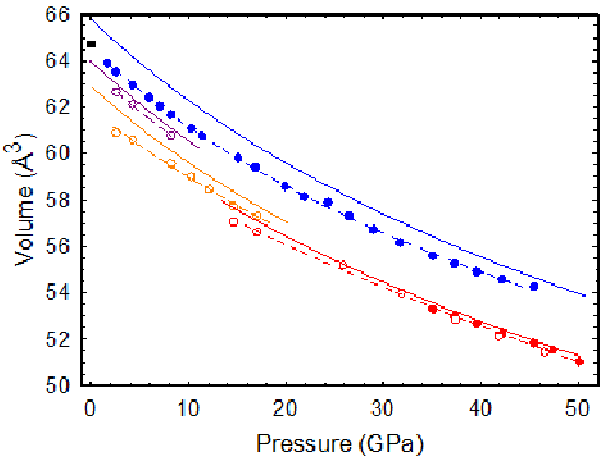

Figure 5. Experimental (circles) and calculated (solid lines) pressure dependences of the volume per formula unit for c-In_2O_3 (blue), rh-In_2O_3 (violet), o3-In_2O_3 (orange), and o1-In_2O_3 (red) phases. Upstroke and downstroke are depicted by full and empty symbols, respectively.

In order to look for candidate structures of the new phase discovered on downstroke, which is intermediate between rh-In_2O_3 and o1-In_2O_3, we resorted to *ab initio* total-energy calculations of a number of structures already found or suggested to occur in ABO_3 compounds, including sesquioxides (*A*=*B*). In particular, we focused in structures which could be intermediate between the R-3c and the Pbcn phases, like the monoclinic P2/c, which was suggested to constitute a diffusionless pathway between both R3-c and Pbcn structures.[29,46] Curiously, our calculations showed that the most competitive phase with the cubic Ia-3, rhombohedral R3-c, and orthorhombic Pbcn phases is not the monoclinic P2/c structure, which follows an enthalpy vs. pressure curve that matches with that of the R-3c phase at all pressures, but the orthorhombic Pbca phase, which is isostructural to Rh_2O_3-III (see Fig. 4).

A good Rietveld refinement (Rwp= 2.8%) of the XRD pattern at 12.1 GPa on downstroke with the Pbca phase (o3-In_2O_3) is shown in Fig. 3. The structure obtained by this refinement was deposited into the FIZ-Karlsruhe database (CSD-number: 426846). **Table 1** shows the experimental values of the lattice parameters and atomic positions for o3-In_2O_3 at 12.1 GPa. Several differences can be noted between the XRD pattern of o3-In_2O_3 and those of o1-In_2O_3 and rh-In_2O_3. o3-In_2O_3 shows a peak below 8º that it is not present in o1-In_2O_3. On the other hand, one broad peak is observed above 9º in o3-In_2O_3, corresponding to several close reflections, while two narrow peaks are observed in rh-In_2O_3. In fact, our XRD pattern at 2.6 GPa on downstroke (see Fig. 2b) can be indexed with a mixture of rh-In_2O_3 (70%) and o3-In_2O_3 (30%). In this respect, we must note that a moderate heating at these conditions resulted in an increase of the proportion of rh-In_2O_3 at the expense of o3-In_2O_3. This information can be helpful for future experiments in order to recover a pure Pbca phase at room conditions.

The unit cell of o3-In_2O_3 (see Fig. 1) contains 8 formula units and all 5 atoms (two In and three O) are in 8c Wyckoff positions. The structure can be understood as a distorted bixbyite-like structure where In is octahedrally coordinated as well as in c-In_2O_3, rh-In_2O_3, and o1-In_2O_3. Octahedral connectivity in the In_2O_3 polymorphs, however, is rather complicated and varies from corner-, through edge-, to face-sharing connections.

A more comprehensive description of the four polymorph structures can be obtained from the analysis of the second-neighbor coordination sphere of metallic atoms.[47-49] In the cation subarray of c-In_2O_3, each In is surrounded by 12 In (d < 3.85 Å) forming a slightly distorted cuboctahedron, like that existing in elemental indium. Furthermore, six of the twelve In – In interatomic distances (4 × 3.35 Å, 2 × 3.37 Å) are comparable to those of metallic In (4 × 3.25 Å, 8 × 3.37 Å), relating the topology and dimensions of oxide and the parent element, as previously reported.[50] At higher pressures, two additional In – In equatorial contacts in the cuboctahedra increase the coordination number to 14 (d < 4.05Å) in o1-In_2O_3. During downstroke, the tendency of the structure is to reduce the number of second neighbors; however, the coordination number in o3-In_2O_3 is also 14 as in o1-In_2O_3, but in a more distorted configuration than in o1-In_2O_3. Finally, after releasing pressure, metastable rh-In_2O_3 shows 13 In – In distances below 4 Å (1 × 2.42 Å corresponding to the face-sharing octrahedra). In summary, the understanding of the four polymorphs on the basis of the second-neighbor coordination is consistent

with the irreversible transformation of metastable rh-In_2O_3 upon heating into the thermodynamically stable c-In_2O_3 at room conditions.

Despite the four RT polymorphs of In_2O_3 up to 50 GPa have sixfold-coordinated In, they have different densities since their unit cell volumes V decrease in the sequence V(Ia-3) > V(R-3c) > V(Pbca) > V(Pbcn), as can be deduced from their equations of state (EOS) plotted in Fig. 5. The corresponding densities for the Ia-3, R-3c, Pbca, and Pbcn phases are 7.179(1) g/cm^3, 7.255(1) g/cm^3, 7.449(1) g/cm^3 and 7.536(1) g/cm^3, respectively. The experimental and theoretical parameters of the EOS of the four polymorphs can be found in **Table 2**.

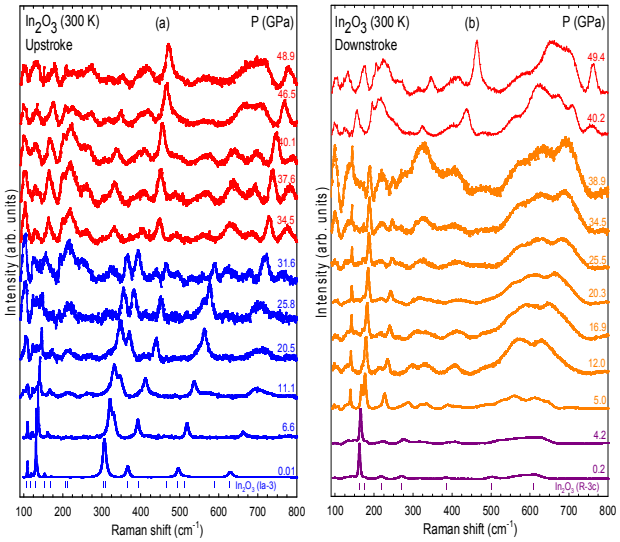

Figure 6. Selected Raman spectra of bulk powder In_2O_3 at different pressures on upstroke up to 50 GPa (a) and on downstroke down to ambient pressure (b). A mixture of 16:3:1 methanol-ethanol-water was used as pressure-transmitting medium. Colours indicate spectra mainly corresponding to cubic Ia-3 (blue), orthorhombic Pbcn (red), orthorhombic Pbca (orange), and rhombohedral R-3c (violet) phases. The frequencies of the main Raman-active peaks of the corundum-type phase at room conditions are indicated in the bottom of figure (b).

The phase transitions on upstroke from c-In_2O_3 to o1-In_2O_3 up to 50 GPa and on downstroke from o1-In_2O_3 to o3-In_2O_3 and from o3-In_2O_3 to rh-In_2O_3, that we have determined by XRD, have been also confirmed by means of RS measurements (see Figs. 6a and 6b). On upstroke, our RS measurements locate the onset of the transformation from c-In_2O_3 to o1-In_2O_3 at 31.6 GPa. Below this pressure, sixteen Raman-active modes of bulk c-In_2O_3 were observed whose frequencies and pressure dependences agree with those recently published.[34] Above 31.6 GPa, new peaks appear and above 34.5 GPa the Raman spectrum already corresponds entirely to o1-In_2O_3. The Raman spectrum of the o1-In_2O_3 is dominated by two well-defined modes at 439 and 719 cm^{-1} (at 31.6 GPa) and by broad bands located in the regions between 180-280, 300-350, and 610-690 cm^{-1}.

On downstroke from 50 GPa, RS measurements show changes in the Raman spectrum below 40 GPa and below 5 GPa. Above 40 GPa, the Raman spectrum corresponds to o1-In_2O_3; however, below this pressure the Raman modes of the new phase appear. In particular, the Raman spectrum of the new phase is dominated by three rather narrow bands around 135, 180, and 240 cm^{-1}, which can be observed down to 5.0 GPa. These modes have been attributed to o3-In_2O_3 since their frequencies and pressure coefficients are consistent with our results from lattice-dynamical *ab initio* calculations. At 5.0 GPa other new Raman peaks appear and at 1.2 GPa the Raman modes of the Pbca phase are no longer seen. The Raman spectra below 1.2 GPa consist of seven Raman modes which match perfectly with those theoretically expected and experimentally measured in rh-In_2O_3 at room conditions.[20] Detailed analysis of the Raman-active modes observed in all the phases (Ia-3, R-3c, Pbca and Pbcn) is out of the scope of the present work and will be reported elsewhere.

In order to understand further the sequence of pressure-induced phase transitions observed in In_2O_3 at RT we performed high-pressure measurements in rh-In_2O_3 samples recovered from pressurizing c-In_2O_3 samples to 50 GPa. RT-XRD measurements at selected pressures up to 25 GPa are shown in Fig.7a. All XRD patterns can be indexed by a mixture of rh-In_2O_3 and o3-In_2O_3. Below 15 GPa, rh-In_2O_3 is dominant while above this pressure it is o3-In_2O_3. On decreasing pressure from 25 GPa to 1 atm the recovered sample was completely in the rh-In_2O_3 phase. This sample was recovered and studied by RT-RS up to 33 GPa (see Fig. 7b). Below 12.4 GPa, only Raman peaks of rh-In_2O_3 are present, while above this pressure new peaks appear that reveal a gradual phase transition with coexistence of both phases till 26 GPa. Between 26 GPa and

33 GPa only Raman modes of o3-In_2O_3 are observed. On decreasing pressure, the rh-In_2O_3 phase is again metastably obtained at room conditions. All these results evidence the good agreement between our XRD and RS data.

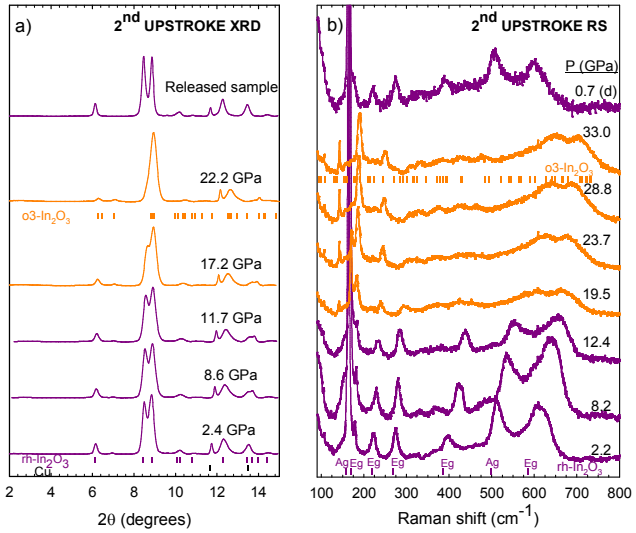

Figure 7. Selected XRD patterns up to 25 GPa (a) and RS spectra up to 33 GPa (b) of rh-In_2O_3. Spectra mainly corresponding to R-3c and Pbca, phases are represented in violet and orange, respectively. Ticks at the bottom of XRD (RS) patterns of 2.4 (2.2) and 22.2 (33.0) GPa mark the positions of the diffraction (Raman) peaks of the dominating rh-In_2O_3 and o3-In_2O_3 phases at each pressure, respectively.

Table 2. Experimental and theoretical values of the unit-cell volume (V_0), bulk modulus (B_0), and pressure derivative (B_0') at room pressure for the three polymorphs c (Ia-3), o1 (Pbcn), and o3 (Pbca) of In_2O_3. Data for the rh (R-3c) phase are not given due to the lack of enough experimental data. Both experimental and theoretical data have been fitted to a second-order Birch-Murnaghan equation of state (B_0' fixed to 4).

Polymorph	Origin	V_0 (Å^3)	B_0 (GPa)	B_0'
c-In_2O_3	Experimental	64.28(13)	184(10)	4.0
	Theoretical	65.72(2)	169.4(12)	4.0
o1-In_2O_3	Experimental	61.9(3)	189(40)	4.0
	Theoretical	62.9(1)	169.6(14)	4.0
o3-In_2O_3	Experimental	61.2(7)	194(10)	4.0
	Theoretical	61.8(2)	185.4(12)	4.0

One question that naturally arises is why the Pbca phase is not observed on upstroke from the Ia-3 phase but it is observed on downstroke from the Pbcn phase. The explanation is still not clear but it is likely that the phase transition from the cubic phase to the Pbca phase at RT is hindered by the presence of a high kinetic energy barrier. This high kinetic energy barrier is present between the cubic phase and the three high-pressure phases (R-3c, Pbca, and Pbcn) as suggested in previous works. In this way, a certain heating is needed to observe the transition to these three high-pressure phases on upstroke and the Pbca was not previously observed in high-pressure high-temperature experiments likely because the right conditions of pressure and temperature were not matched. On the other hand, if the barriers between the three high-pressure phases are not so high the transformation between the three of them can be experimentally observed on downstroke at RT from the original Pbcn phase.

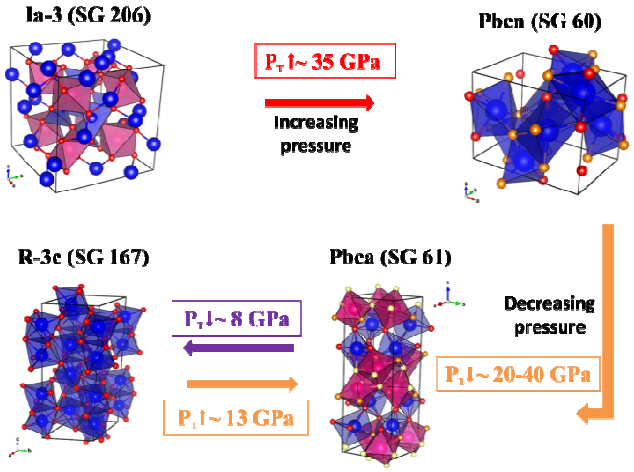

Scheme 1. Sequence of pressure-induced phase transitions in In_2O_3 up to 50 GPa. Atoms in different Wyckoff sites are depicted by different colors: In (blue and pink) and O (red, yellow and orange).

To sum up the results obtained in this work, Scheme 1 displays the sequence of pressure-induced phase transitions in In_2O_3 at RT up to 50 GPa. In this work, the four known polymorphs of In_2O_3 with the same coordination for In atoms were obtained starting from the cubic polymorph by compression and decompression at RT. To our knowledge, it is the first time that this phenomenon has been observed. We want to comment that the scheme of pressure-induced phase transitions here proposed for In_2O_3 at RT is in disagreement with many previous reports and prompts for a revision of previous results. As already commented, the observed phase transition from c-In_2O_3 to 01-In_2O_3 above 35 GPa is in disagreement with previous results which suggested that the R-3c phase is the post-cubic phase.[32,33] A careful analysis of XRD peaks assigned by Liu et al.[32] and Qi et al.[33] to the R-3c phase suggests the possibility to assign them also to the Pbcn phase. Note that data of the high-pressure phase reported by Liu et al. and Qi et al. show no XRD peak at small angles, as we have already commented we have observed for the Pbcn phase. Therefore, we think that these authors already found the phase transition from c-In_2O_3 to 01-In_2O_3, even at smaller pressures than in this work likely due to the presence of slightly non-hydrostatic conditions in their experiments. We also want to note that RS data of the high-pressure phase reported by Liu et al. are not consistent with the R-3c phase, as it was already commented by García-Domene et al.[34] In fact, if the XRD data of Qi et al.[33] are reinterpreted on this basis, these authors indeed provided evidence for the metastable recovery of the 01-In_2O_3 at room pressure at least in nanocrystals.

On the other hand, the observed phase transition from rh-In_2O_3 to 03-In_2O_3 above 12 GPa is apparently in disagreement with results of Gurlo et al. who pointed out that no phase transition was observed in rh-In_2O_3 up to 30 GPa at RT.[28] Nevertheless, a close analysis of the RT-XRD patterns reported by these authors at 24 and 30 GPa show that they are quite different from those of the rh-In_2O_3 at room pressure and that they exhibit similarities with those of the 03-In_2O_3 structure shown in this work. However, our results and those of Gurlo et al. could be slightly different because, unlike us, they used nanocrystalline rh-In_2O_3 powder in their high-pressure study. Finally, we have to note that Bekheet et al. have recently reported the stabilization of an orthorhombic phase of In_2O_3 at 1 atm after pressurizing rh-In_2O_3 at 9 GPa and 600ºC.[29] These authors have identified it as the 01-In_2O_3 phase; however, our results suggest the 03-In_2O_3 phase could be indeed recovered as a metastable phase at 1 atm since its enthalpy is even smaller than that of 01-In_2O_3 at ambient pressure. Therefore, further studies are needed to fully understand the structural HP-HT behavior of In_2O_3. We hope the results here reported will trigger such studies.

CONCLUSIONS

We report the discovery of a new polymorph of In_2O_3 at high pressures. The new polymorph (03-In_2O_3) crystallizes in the Rh_2O_3-III structure and has been found to be the post-corundum phase; i.e., the high-pressure phase between the R-3c and Pbcn phases. This discovery has far-reaching implications for the understanding of the pressure-temperature diagram of In_2O_3 and of other sesquioxides. The Pbca space group was previously found only as a high-temperature phase of Rh_2O_3 (Rh_2O_3-III).[13] Other sesquioxides have been found in this space group. This is the case of the poorly-known α-Mn_2O_3,[51] which is not isostructural to Rh_2O_3-III, and which has been recently postulated to be the low-temperature phase of Mn_2O_3.[52] Another case is mineral "panguite", recently found in the Allende meteorite[53] and mainly composed of Ti_2O_3. This mineral belongs to the Pbca space group but again it is not isostructural to Rh_2O_3-III. These results show that struc-

tures belonging to the Pbca space group are the less known and understood phases of sesquioxides and that they could be found in other corundum-type sesquioxides. In fact, our preliminary calculations indicate that the Rh_2O_3-III phase could be relevant in other corundum-type sesquioxides, like Al_2O_3, Ga_2O_3, V_2O_3, Cr_2O_3, and Fe_2O_3 at high pressures. Therefore, we stress that detailed experimental studies on upstroke and downstroke should be performed to confirm its presence in other sesquioxides.

AUTHOR INFORMATION

Corresponding Author

* juasant2@upv.es, Tel: (+34)963575269

ACKNOWLEDGMENT

Financial support by the Spanish MEC under Grant No. MAT2010-21270-C04-01/03/04, MAT2013-46649-C4-1/2/3-P, by MALTA Consolider Ingenio 2010 project (CSD2007-00045) and by Generalitat Valenciana (GVA-ACOMP-2013-012). Red Española de Supercomputación (RES) and ALBA Synchrotron Light Source are also acknowledged. BGD and JAS acknowledge financial support through the FPI program and Juan de la Cierva fellowship. We also thank J. L. Jordá for fruitful discussions. ALJP acknowledge financial support through Brazilian CNPq. AS thanks to FEDER grant UNLV10-3E-1253 for financial support.

REFERENCES

(1) Takada T.; Suzuki K.; and Nakane M. Highly sensitive ozone sensor. *Sensors and Actuators B-Chemical* **1993**, 13, 404-407.

(2) Favier F.; Walter E. C.; Zach M. P.; Benter T.; and Penner R. M. Hydrogen Sensors and Switches from Electrodeposited Palladium Mesowire Arrays. *Science* **2001**, 293, 2227-2231.

(3) Gurlo A. Nanosensors: towards morphological control of gas sensing activity. SnO_2, In_2O_3, ZnO and WO_3 case studies. *Nanoscale* **2011**, 3, 154-165.

(4) Lan J. L.; Lin Y. H.; Liu Y.; Xu S. L.; and Nan C.W. High Thermoelectric Performance of Nanostructured In_2O_3-Based Ceramics. *J. Am. Cer. Soc.* **2012**, 95, 2465-2469.

(5) Sootsman J. R.; Chung D. Y.; and Kanatzidis M. G. New and Old Concepts in Thermoelectric Materials. *Angew. Chem. Int. Ed.* **2009**, 121: 8768-8792; *Angew. Chem. Int. Ed.* **2009**, 48, 8616-8639.

(6) Burroughes J. H.; Bradley D. D. C.; Brown A. R.; Marks R. N.; Mackay K.; Friend R. H.; Burns P. L.; and Holmes A. B. Light-emitting diodes based on conjugated polymers. *Nature* **1990**, 347, 539-541.

(7) Hsu S. F.; Lee C. C.; Hwang S. W.; and Chen C. H. Highly efficient top-emitting white organic electroluminescent devices. *Appl. Phys. Lett.* **2005**, 86, 253508.

(8) Kaspar T. C.; Droubay T.; and Jaffe J. E. ZnO/Sn:In2O3 and ZnO/CdTe band offsets for extremely thin absorber photovoltaics. *Appl. Phys. Lett.* **2011**, 99, 263504.

(9) Ellmer K. Past achievements and future challenges in the development of optically transparent electrodes. *Nat. Photonics* **2012**, 6, 809-817.

(10) Shannon R. D. New high pressure phases having the corundum structure. *Solid State Commun.* **1966**, 4, 629-630.

(11) Prewitt C. T.; Shannon R. D.; Rogers D. B.; and Sleight A. W. rare earth oxide-corundum transition and crystal chemistry of oxides having the corundum structure. *Inorg. Chem.* **1969**, 8, 1985.

(12) Atou T.; Kusaba K.; Fukuoka K.; Kikuchi M.; and Syono Y. Shock-induced phase transition of M_2O_3 (M = Sc, Y, Sm, Gd, and In)-type compounds. *J. Solid State Chem.* **1990**, 89, 378-384.

(13) Christensen A. N.; Broch N. C.; Heidenstam O.; and Nilsson A. Hydrothermal Investigation of the Systems In_2O_3-H_2O-Na_2O and In_2O_3-D_2O-Na_2O. The Crystal Structure of Rhombohedral In_2O_3 and of $In(OH)_3$. *Acta Chem. Scand.* **1967**, 21, 1046-1056.

(14) Yu D.; Yu S.-H.; Zhang S.; Zuo J.; Wang D.; and Qian Y. Metastable Hexagonal In2O3 Nanofibers Templated from InOOH Nanofibers under Ambient Pressure. *Adv. Funct. Mater.* **2003**, 13, 497-501.

(15) Gurlo A.; Ivanovskaya M.; Barsan N.; and Weimar U. Corundum-type indium (III) oxide: formation under ambient conditions in Fe_2O_3-In_2O_3 system. *Inorg. Chem. Commun.* **2003**, 6, 569-572.

(16) Epifani M.; Siciliano P.; Gurlo A.; Barsan N.; and Weimar U. Ambient Pressure Synthesis of Corundum-Type In_2O_3. *J. Am. Chem. Soc.* **2004**, 126, 4078-4079.

(17) Yu D.; Wang D.; and Qian Y. Synthesis of metastable hexagonal In_2O_3 nanocrystals by a precursor-dehydration route under ambient pressure. *J. Solid State Chem.* **2004**, 177, 1230-1234.

(18) Sorescu M.; Diamandescu L.; Tarabasanu-Mihaila D.; and Teodorescu V. S. Nanocrystalline rhombohedral In_2O_3 synthesized by hydrothermal and post-annealing pathways. *J. Mater. Sci.* **2004**, 39, 675-677.

(19) Xu J. Q.; Chen Y. P.; Pan Q. Y.; Xiang Q.; and Dong X. W. A new route for preparing corundum-type In_2O_3 nanorods used as gas-sensing materials. *Nanotechnol.* **2007**, 18, 115615.

(20) Wang Ch.-Y.; Dai Y.; Pezoldt J.; Lu B.; Kups Th.; Cimalla V.; and Ambacher O. Phase Stabilization and Phonon Properties of Single Crystalline Rhombohedral Indium Oxide. *Cryst. Growth & Design* **2008**, 8, 1257-1260.

(21) King P. D. C.; Veal T. D.; Fuchs F.; Wang Ch.-Y.; Payne D. J.; Bourlange A.; Zhang H.; Bell G. R.; Cimalla V.; Ambacher O.; Egdell R. G.; Bechstedt F.; and McConvill C. F. Band gap, electronic structure, and surface electron accumulation of cubic and rhombohedral In_2O_3. *Phys. Rev. B* **2009**, 79, 205211.

(22) Murakami M.; Hirose K.; Kawamura K.; Sata N.; and Ohishi Y. Post-Perovskite Phase Transition in $MgSiO_3$. *Science* **2004**, 304, 855-858.

(23) Karazhanov S. Zh.; Ravindran P.; Vajeeston P.; Ulyashin A.; Finstad T. G.; and Fjellvag H. Phase stability, electronic structure, and optical properties of indium oxide polytypes. *Phys. Rev. B* **2007**, 76, 075129.

(24) Caracas R.; and Cohen R. E. Post-perovskite phase in selected sesquioxides from density-functional calculations. *Phys. Rev. B* **2007**, 76, 184101.

(25) Yusa H.; Tsuchiya T.; Sata N.; and Ohishi Y. Rh2O3(II)-type structures in Ga_2O_3 and In_2O_3 under high pressure: Experiment and theory. *Phys. Rev. B* **2008**, 77, 064107.

(26) Yusa H.; Tsuchiya T.; Tsuchiya J.; Sata N.; and Ohishi Y. α-Gd_2S_3-type structure in In_2O_3: Experiments and theoretical confirmation of a high-pressure polymorph in sesquioxide. *Phys. Rev. B* **2008**, 78, 092107.

(27) Gurlo A.; Kroll P.; and Riedel R. Metastability of Corundum-Type In_2O_3. *Chem. Eur. J.* **2008**, 14, 3306-3310.

(28) Gurlo A.; Dzivenko D.; Kroll P.; and Riedel R. High-pressure high-temperature synthesis of Rh2O3-II-type In_2O_3 polymorph. *Phys. Stat. Sol. (RRL)* **2008**, 2, 269-271.

(29) Bekheet M. F.; Schwarz M. R.; Lauterbach S.; Kleebe H.-J.; Kroll P.; Riedel R.; and Gurlo A. Orthorhombic In_2O_3: A Metastable Polymorph of Indium Sesquioxide. *Angew. Chem. Int. Ed.* **2013**, 52, 6531-6535.

(30) Walsh A.; and Scanlon D. O.) Polymorphism of indium oxide: Materials physics of orthorhombic In_2O_3. *Phys. Rev. B* **2013**, 88, 16120(R).

(31) Umemoto K.; and Wentzcovitz R. M. Effect of the d electrons on phase transitions in transition-metal sesquioxides. *Phys. Chem. Minerals* **2011**, 38, 387-395.

(32) Liu D.; Lei W. W.; Zou B.; Yu S. D.; Hao J.; Wang K.; Liu B. B.; Cui Q. L.; and Zou G. T. High-pressure x-ray diffraction and Raman spectra study of indium oxide. *J. Appl. Phys.* **2008**, 104, 083506.

(33) Qi J.; Liu J. F.; He Y.; Chen W.; and Wang C. Compression behavior and phase transition of cubic In_2O_3 nanocrystals. *J. Appl. Phys.* **2011**, 109, 063520.

(34) García-Domene B.; Ortiz H. M.; Gomis O.; Sans J. A.; Manjón F. J.; Munoz A.; Rodríguez-Hernández P.; Achary S. N.; Errandonea D.; Martínez-García D.; Romero A. H.; Singhal A.; and Tyagi A. K. High-pressure lattice dynamical study of bulk and nanocrystalline In_2O_3. *J. Appl. Phys.* **2012**, 112, 123511.

(35) Biesterbos J. W. M.; Hornstra J.; and Less J. The crystal structure of the high-temperature, low-pressure form of Rh_2O_3. *Common Metals* **1973**, 30, 121-125.

(36) Bekheet M. F.; Schwarz M. R.; Lauterbach S.; Kleebe H. J.; Kroll P.; Stewart A.; Kolb U.; Riedel R.; and Gurlo A. In situ high pressure high temperature experiments in multi-anvil assemblies with bixbyite-type In_2O_3 and synthesis of corundum-type and orthorhombic In_2O_3 polymorphs. *High Press. Res.* **2013**, 33, 697-711.

(37) Dewaele A.; Loubeyre P.; and Mezouar M. Equations of state of six metals above 94GPa. *Phys. Rev. B* **2004**, 70, 094112.

(38) Fauth F.; Peral I.; Popescu C.; and Knapp M. The new Material Science Powder Diffraction beamline at ALBA Synchrotron. *Powder Diffraction* **2013**, 28; S360-S370.

(39) Kraus W.; and Nolze G. POWDER CELL - a program for the representation and manipulation of crystal structures and calculation of the resulting X-ray powder patterns. *J. Appl. Cryst.* **1996**, 29, 301-303.

(40) Toby B. H. EXPGUI, a graphical user interface for GSAS. *J. Appl. Cryst.* **2001**, 34, 210-213.

(41) Syassen K. Ruby under pressure. *High Pres. Res.* **2008**, 28, 75-126.

(42) Kresse G.; and Hafner J. Ab initio molecular dynamics for liquid metals. *Phys. Rev. B* **1993**, 47, 558-561.

(43) Kresse G.; and Hafner J. Ab initio molecular-dynamics simulation of the liquid-metal amorphous-semiconductor transition in germanium. *Phys. Rev. B* **1994**, 49, 14251-14269.

(44) Kresse G.; and Furthmuller J. Efficiency of ab-initio total energy calculations for metals and semiconductors using a plane-wave basis set. *Comput. Mater. Sci.* **1996**, 6, 15-50.

(45) Kresse G.; and Furthmuller J. Efficient iterative schemes for ab initio total-energy calculations using a plane-wave basis set. *Phys. Rev. B* **1996**, 54, 11169-11186.

(46) Xu B.; Stokes H.; and Dong J.J. First-principles calculation of kinetic barriers and metastability for the corundum-to-Rh_2O_3(II) transition in Al_2O_3. J. Phys.: Condens. Matter **2010**, 22, 315403.

(47) Martínez-Cruz L. A.; Ramos-Gallardo A.; and Vegas A. MSn and $MSnO_3$ (M = Ca, Sr, Ga): new examples of oxygen-stuffed alloys. *J. Solid State Chem.* **1994**, 110, 397-398.

(48) Vegas A.; and Jansen M. Structural relationships between cations and alloys; an equivalence between oxidation and pressure. *Acta Cryst. B* **2002**, 58, 38-51.

(49) Santamaría-Pérez D.; and Chuliá-Jordán R. Compression of mineral barite, $BaSO_4$: a structural study. *High Press. Res.* **2012**, 32, 81-88.

(50) Vegas A. Cations in inorganic solids. *Crystallogr. Rev.* **2000**, 7, 189-283.

(51) Geller S. Structure of α-Mn_2O_3, $(Mn_{0.983}Fe_{0.017})_2O_3$ and $(Mn_{0.37}Fe_{0.63})_2O_3$ and relation to magnetic ordering. *Acta Cryst. B* **1971**, 27, 821-828.

(52) Ovsyannikov S. V.; Abakumov A. M.; Tsirlin A. A.; Schnelle W.; Egoavil R.; Verbeeck J.; Van Tendeloo G.; Glazyrin K. V.; Hanfland M.; and Dubrovinsky L. Perovskite-like Mn_2O_3: A Path to New Manganites. *Angew. Chem. Int. Ed.* **2013**, 52, 1494-1498.

(53) Ma C.; Tschauner O.; Beckett J. R.; Rossman G. R.; and Liu W. J. Panguite, $(Ti^{4+},Sc,Al,Mg,Zr,Ca)_{1.8}O_3$, a new ultra-refractory titania mineral from the Allende meteorite: Synchrotron micro-diffraction and EBSD. *American Mineralogist* **2012**, 97, 1219-1225.

SYNOPSIS TOC.